López, JJ.; Martín, J.; García Martínez, A.; Villalta-Lara, D.; Warey, A. (2017). Implementation of two color method to investigate late cycle soot oxidation process in a CI engine under low load conditions. Applied Thermal Engineering. 113:878-890. doi:10.1016/j.applthermaleng.2016.11.095

Implementation of Two Color Method to Investigate Late Cycle Soot Oxidation Process in a CI Engine under Low Load Conditions

Authors:

J. Javier López[1], Jaime Martín[1], Antonio García[1], David Villalta[1]

Alok Warey[2]

Affiliation:

1. CMT Motores Térmicos – Universitat Politècnica de València, Camino de Vera s/n, 46022, Valencia, Spain.
2. Propulsion Systems Research Lab, General Motors Global Research and Development.

Corresponding Author:

Dr. Antonio García

CMT - Motores Térmicos /Universitat Politècnica de València

angarma8@mot.upv.es

HIGHLIGHTS

High uncertainties in flame transparency are obtained for high load conditions

The half-life time is a good estimator to characterize the soot oxidation process

If injection pressure is reduced, the soot oxidation process is decreased

Lower the ambient density and/or temperature, larger the mixing capability

The soot oxidation process is explained by the mixing process and bulk temperature

ABSTRACT

Soot emissions from diesel engines are an important concern in meeting emissions regulations. Soot emissions are the result of two competing processes: soot formation and soot oxidation. Mechanisms of soot formation are discussed extensively in the literature. Equivalence ratio at lift-off length along with residence time and gas temperature play an important role for soot formation in a diffusion flame. Mixing capability and bulk gas temperature are the most important parameters that influence the in-cylinder soot oxidation process. Normally, research studies of soot formation-oxidation processes have been developed under controlled and not completely representative conditions of engine operation in the field. Therefore, the main objective of this work was to develop a simplified methodology to evaluate in-cylinder soot oxidation under 'real' engine conditions. In particular, the impact of mixing process and bulk gas temperature on late cycle soot oxidation was evaluated. The experimental measurements were made in a production light-duty diesel engine varying those parameters that have been demonstrated in the literature as the most relevant in soot formation – oxidation processes; injection pressure, ambient density and intake air temperature. To measure soot, two color method was applied by means of an

optoelectronic pyrometer. To evaluate the mixing capability a specific “tracer” Apparent Combustion Time (ACT^{-1}) based on the experimental heat release and injection parameters was defined. The relationship between both parameters was used to explain the soot oxidation process.

KEYWORDS

Multi-cylinder pyrometer, soot oxidation, two color method, optical thickness, mixing capability

1. INTRODUCTION

Internal Combustion Engines (ICE) are the most widely used technology in automotive sector. In particular, the Direct-Injection (DI) diesel engine is identified as the most efficient powertrain due to lower fuel consumption compared to Spark Ignition (SI) engines. This benefit has been supported by extensive research in different fields: in-cylinder heat transfer (HT) reduction [1], improvement in thermal management [2], reduction of friction and auxiliaries losses [3], and indicated cycle optimization [4], among others. In spite of its high efficiency, diesel engines have two area of focus: emissions of nitrogen oxides (NOx) and particulate matter (PM), with soot being a major component. These two pollutants are regulated by emissions legislations and thus, engine designers are motivated to develop new combustion strategies for reducing the engine-out pollutant emissions [5, 6].

Focusing on soot emissions it is possible to state that soot production in a diesel engine is the result of two competing processes: soot formation and soot oxidation. Thus, spatially the first soot precursors are formed in the fuel-rich premixed burn region in the diffusion flame depending on the local equivalence ratio [7, 8, 9]. Once these precursors

appear, particle growth occurs due to high temperature and absence of oxygen in the region covered by the diffusion flame. Now, regarding the soot oxidation process, two different stages in the temporal evolution of the in-cylinder soot concentration need to be considered [10]: in the first stage, from the Start of Injection (SoI) up to the End of Injection (EoI), a quasi-steady state is achieved, and nearly all the soot formed in the spray core is oxidized when reaches the diffusion flame front. In the second stage, from EoI up to the End of Combustion (EoC), the diffusion flame vanishes and soot formation decreases. At these conditions soot oxidation is strongly coupled with the mixing rate and the in-cylinder temperature [8]. It is also worthy to note that only a small fraction of the soot formed in cylinder is emitted in the exhaust [11]. The soot formation process has been studied extensively [12], but now we are going to focus on some studies on in-cylinder soot oxidation that can be highlighted. Pickett et al. [7], reported that a reduction in the in-cylinder ambient density causes a large decrease in the peak soot volume fraction due to longer combustion duration and slower combustion development. Measurements were made by using laser extinction under a wide range of operating conditions. Gallo et al. [13], using an optical diesel engine, demonstrated that a reduction in oxygen concentration results in a decrease in in-cylinder soot oxidation. In their study, time resolved extinction measurements have been used to estimate soot oxidation rates during the expansion stroke. Dembinski et al. [14] analyzed the impact of increased turbulence, caused by higher injection pressure and higher swirl number, on in-cylinder soot oxidation. These authors concluded that the soot oxidation process is enhanced with turbulence. Tree and Svensson [9] studied the effect of different engine parameters on the soot oxidation process, concluding that the ambient temperature had the greatest effect by increasing the reaction rates. In addition, Huestis et al. [15] analyzed the in-cylinder processes and exhaust emissions,

using two-color pyrometry in combination with soot concentration measurements in the exhaust. Natural luminosity from the flame was collected using three photo diodes with different band pass filters. These authors concluded that a drastic decrease in the oxygen intake concentration (up to 9%) implies a monotonic decrease in the cycle soot oxidation rate [15], which is consistent with the results reported in [13]. Using a similar optical approach, Lopez et al. [16] also studied the in-cylinder soot oxidation process by means of the two-color method. In particular, the impact of swirl, EGR and injection timing were analyzed. These authors concluded that the soot oxidation process is degraded when swirl is decreased, EGR rate is increased or injection timing is delayed.

Thus, the main objective of this work is to define a simplified methodology to evaluate the in-cylinder soot oxidation under real engine conditions. In particular, the impact of the mixing process and bulk gas temperature on soot oxidation will be evaluated. The experimental measurements will be made in a production light-duty diesel engine varying those parameters that have been demonstrated in the literature as being the most relevant in the soot formation – oxidation processes: injection pressure, ambient density and intake air temperature. To measure soot, the two color method will be applied by means of an optoelectronic pyrometer. To evaluate the mixing capability, a specific "tracer" (ACT^{-1}) based on both the experimental heat release and the injection profiles will be defined. The relationship between both parameters will be used to explain the soot oxidation process.

2. EXPERIMENTAL SET UP

2.1. Multi-cylinder Light Duty Engine

The engine used in the present research was a production-type GM 1.9L 4-cylinder diesel engine, equipped with a common-rail fuel injection system, a variable geometry

turbocharger (VGT), an intake throttle valve able to modify the swirl number (swirl flap) and a high pressure exhaust gas recirculation system. The engine had four valves per cylinder, allowing centrally located injectors, and a re-entrant type piston bowl. The swirl ratio could be varied from 1.4 up to 3 thanks to the dedicated swirl flap mentioned previously. The most relevant engine data as well as the main specifications of the injection system are given in Table 1.

Engine Type	DI, 4-cylinder,turbocharged,4-stroke
Displaced volume	1900 cc
Stroke	90.4 mm
Bore	82 mm
Piston Bowl	Re-entrant type
Compression ratio	17.5:1
Max. Power [kW]	110 @4000rpm
Max. Torque [Nm/min^{-1}]	320 / 2000-2750
Injection System	Bosch Common Rail (solenoid)
Max. Rail Pressure [bar]	1600
Nozzle hole diameter [mm]	0.141
Injector Nozzle Holes	7

Table 1. Engine and injection system specifications

The engine was coupled to an electric dynamometer allowing the control of both the engine speed and load. The test bench also included complete instrumentation to measure different fluid temperatures and mass flow rates.

The in-cylinder pressure, which is a vital parameter for the combustion process analysis in the frame of the present research, was measured for each cylinder and 100 consecutive cycles with Kistler 6125C10 piezoelectric pressure transducers and Kistler 4603B10 charge amplifiers. This pressure was sampled every 0.5° by a DRIVVEN engine controller [17]. The mean variables were acquired at a low sampling frequency of 100 Hz using SAMARUC, a CMT-developed test system that collects the signals of different sensors and controls the electric dynamometer [18].

2.2. Test Matrix

The engine was operated maintaining constant engine speed at 2000 rpm. Considering flame transparency drawbacks imposed by the two color method (described in appendix) used to measure optical thickness (KL), the study was focused on low load conditions. In particular, to cases at 2 and 5 bar BMEP, respectively, were selected with the goal of characterizing the soot oxidation process. For that purpose, three different engine variables were swept: injection pressure, intake air temperature and in-cylinder density. In the case of injection pressure, a sweep from 400 bar to 800 bar was performed, the intake temperature was kept constant at 318 K and the ambient density at Top Dead Center (TDC) was maintained constant at 20.3 kg/m^3 and 23.2 kg/m^3 depending on the engine load. Concerning the sweep of the ambient density at TDC, the range of values were defined considering the minimum, middle and maximum intake pressure produced by the turbocharger for each operating point. The injection pressure was 450 bar for the 2 bar BMEP case and 650 bar for the 5 bar BMEP case. The intake temperature was not changed independently of the engine load at 313 K. Finally, an additional sweep of the air intake temperature was performed maintaining constant the ambient density at TDC at 22 kg/m^3 for both engine loads. With this objective, different intake pressures were used, from 1.24 bar to 1.33 bar (absolute). The injected fuel mass was kept constant for each load (9.8 mg/cc for the 2 bar BMEP cases and 17.8 mg/cc for 5 bar BMEP cases). For all the engine conditions measured, a single injection strategy (main injection only) was used, with the different injection timings shown in Table 2. A swirl ratio of 1.4, a CA50 of 13 Crank Angle Degrees (CAD) after TDC (aTDC) and no EGR were used. Table 2 presents the test matrix for the two engine operating conditions used in this study.

	bmep [bar]	Injection Timing [µs]	Intake press. [bar]	Exhaust press. [bar]	Air mass [kg/min]	P_{inj} [bar]	Density [kg/m^3]	Intake Temp. [K]
Injection Pressure	2	777, 621, 544	1.17	1.28	2.29	400, 600, 800	20.3	318
	5	995, 777, 671	1.36	1.48	2.64	400, 600, 800	23.2	
Ambient Density	2	715	1.03 / 1.26 / 1.48	1.10 / 1.51 / 2.41	2.04 / 2.49 / 2.88	450	18.1 / 22 / 25.6	313
	5	750	1.07 / 1.37 / 1.65	1.13 / 1.57 / 2.61	2.11 / 2.71 / 3.20	650	18.5 / 23.5 / 28.1	
Intake Air Temperature	2	715	1.24 / 1.27 / 1.31 / 1.36	1.24 / 1.26/ 1.30 / 1.33	2.53 / 2.53 / 2.54 / 2.57	450	22	303 / 313 / 323 / 333
	5	750		1.24 / 1.26/ 1.30 / 1.33		650		

Table 2. Experimental engine operating conditions

Commercially available European diesel fuel was used in this study.

2.3. Optoelectronic Pyrometer

The in-cylinder soot measurements were performed with an optoelectronic signal converter with a selection of photodiodes and narrow band optical filters adapted to specific applications for combustion engine flame and soot measurements. This light probe was developed by AVL and is known as VisioFEM. A sapphire lens at the tip of the probe captures the light from the combustion chamber with a view angle of 90º. The soot radiation is transmitted through optical fibers and split to two filters at wavelengths λ_1=600 and λ_2=950 nm (with ± 50nm FWHM), respectively. Then, the photodiodes convert the intensity to a voltage signal. The signals from the photodiodes are amplified and recorded every 0.5°CAD. Figure 1 shows a scheme of the optoelectronic probe. Signal conversion and conditioning ensures the highest as possible linearity of the input radiation intensity to the output signal voltage. The Optoelectronic raw signals and the absolute light intensities are linked by a calibration of the whole measurement chain using a halogen lamp, which provides a homogenously illuminated surrounding. At

each operating point, once the engine is stabilized, 400 combustion cycles (4 repetitions of 100 cycles) are recorded.

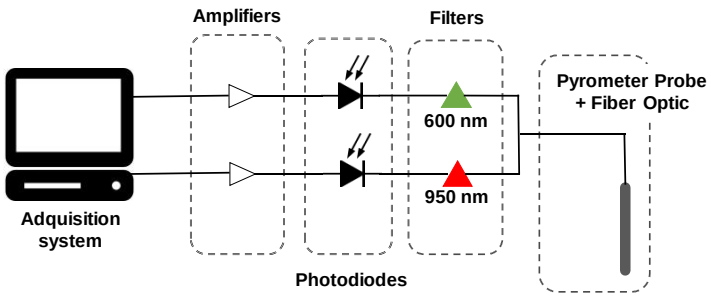

Figure 1. Signal path from flame to data acquisition device

Once the transmission is determined, the spectral emission is calculated by Equation 1:

$$I_{soot}\left[\frac{W}{m^2 \cdot m \cdot sr}\right] = \frac{Voltage\ signal\ [V] \cdot Sensitivity\ [\frac{W}{m^2 \cdot m \cdot sr \cdot V}]}{Gain \cdot Transmission} \qquad (1)$$

where I_{soot} is spectral emission, voltage signals are measured at 600 and 950 nm, sensitivity constants are provided by pyrometer manufacturer and the gain is selected depending on the light intensity to avoid saturation.

Once spectral emission is obtained with the optoelectronic pyrometer, the two color method is applied for calculating the soot temperature and KL. KL represents the "cumulated" soot volume fraction. In particular, K is the dimensional coefficient of the soot cloud (proportional to the soot volume fraction) an L is the path length, which corresponds to the size of the cloud in the direction of the line-of-sight. This technique indicates that the intensity of radiation emitted by soot particles (I_{soot}) is proportional to the radiation emitted by a black body at the same temperature (T). This proportionality is determined by the emissivity of the particles, which can be expressed in terms of soot concentration, working wavelength (λ) and a constant parameter (α) [19]. Therefore, I_{soot} can be expressed as the following equation:

$$I_{soot}(\lambda, T, KL) = \varepsilon_\lambda I_{b,\lambda} = \left[1 - exp\left(-\frac{KL}{\lambda^\alpha}\right)\right] \frac{1}{\lambda^5} \frac{c_1}{\left[exp\left(\frac{c_2}{\lambda T}\right) - 1\right]} \qquad (2)$$

where c_1 = 1.1910439 x 10^{-16} Wm^2sr^{-1} and c_2 = 1.4388 x 10^{-2}mK. Zhao et al. [20] reported that α values are less dependent on the wavelength in the visible range than in the infrared. In this study α was assumed to be 1.39, which is a value commonly used for most of the fuels [21].

For the sake of clarity, figure 2 presents the optical set up when the optoelectronic pyrometer is used in the light duty engine. In this figure, the piston is located at 20 CAD after top dead center. It is possible to observe the injector, the optoelectronic flush mounted probe as well as its field of vision in the combustion chamber.

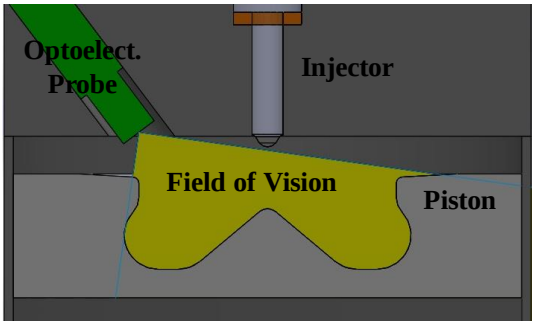

Figure 2. Optoelectronic pyrometer set up on the light duty engine configuration.

3. THEORETICAL TOOLS

3.1. Apparent Combustion Time Concept

To estimate mixing capability an Apparent Combustion Time (ACT) parameter was used [22]. This parameter was calculated as shown in Figure 3 (for a particular case with a single injection): it is the dwell time between the instant where a certain percentage of the mass of fuel has been injected (point of injection, POI_i) and the instant where this same percentage is burned (point of combustion, POC_i). On the one hand,

this fact does not imply that all the fuel injected in a given instant burns after the ACT_i: this parameter is just representative of the time necessary for a percentage of injected fuel to be ready for combustion. On the other hand, the ACT must not be confused with the ignition delay, because the ACT has a more general meaning: only the ACT corresponding to the first injected fuel coincides with the ignition delay (as shown in Figure 3) whereas it has a certain evolution for the rest of the injected fuel. This evolution is shown in Figure 4, where the ACT parameter (black solid line) corresponding to the case presented in Figure 3 has been plotted. As it is possible to observe in Figure 4, the ACT^{-1} parameter is also plotted. In this sense ACT^{-1} is considered as a mixing capability tracer. Thus, it is possible to observe how the mixing capability remains almost constant while the injection is in progress (up to a mass fraction of 0.43), since it is the momentum flux introduced by the nozzle which governs the mixing process. Nonetheless, once the end of injection is reached, the mixing capability starts to decrease, tending to its lowest value at the end of the combustion process.

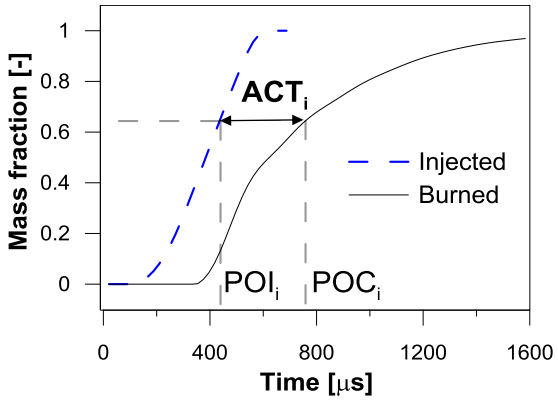

Figure 3. Definition for the Apparent Combustion Time (ACT).

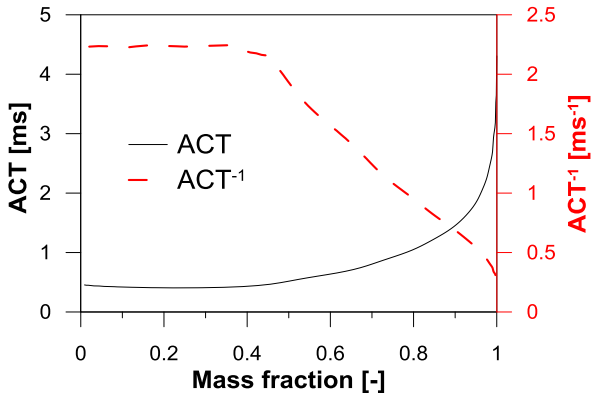

Figure 4. Evolution of the ACT and ACT^{-1} parameter for the case shown in Figure 3 (single injection pulse).

3.2. In-cylinder pressure signal analysis: CALMEC

The combustion analysis was performed by means of an in-house tool named CALMEC, which is comprehensively described in [23]. The main input for the combustion diagnosis is the in-cylinder pressure signal, which is measured from 100 consecutive engine cycles in order to reduce the effect of the cycle-to-cycle variation on the results uncertainty. The raw pressure data was smoothed using a low-pass filter and then averaged in order to yield a representative in-cylinder pressure trace, which was used to perform the analysis. Then, the first law of thermodynamics was applied during the closed cycle (from IVC to EVO), assuming that the combustion chamber is as an open system due to the blow-by leakage and the fuel injection. Ideal gas law was used to calculate the mean gas temperature in the chamber from the pressure and the instantaneous mass. The main outcome of the model used for the analysis is the rate of heat release (RoHR) along with some derived parameters such as the start of combustion (defined as the crank angle in which the cumulated heat release reaches 2% of the fuel energy) and the combustion centering (defined as the crank angle at which 50% of the fuel mass is burned), among other parameters.

3.3. KL and ACT^{-1} half-life times

Figure 5 shows the temporal evolution of the experimental average KL together with its standard deviation for the 2000 rpm and 2 bar BMEP case with an injection pressure of 400 bar. In addition, the EoI is marked with a vertical dashed straight line. The KL profile can be split in two parts. The first part consists of the period from SoI up to EoI. It can be checked that during the fuel injection process the soot balance is governed mainly by the formation process and therefore the KL increases. The second part consists of late-cycle combustion, from EoI up to EoC. The fuel injection process is completed and thus, the soot formation phenomenon starts to be mitigated. Then, the soot oxidation begins to be the principal mechanism which rules the soot balance. In spite of significant soot oxidation during the first part, only the second part is considered for calculation of KL half-life time in this study, since the oxidation during this part is the main responsible for the final engine-out soot emissions.

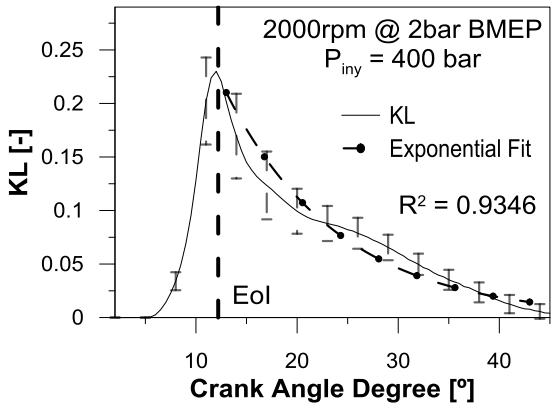

Figure 5. KL trace for the P_{inj} = 400 bar case at point 2000rpm@2bar BMEP and its exponential fit

Assuming that the last part of the curve (from EoI up to EoC) presented in Figure 5 follows an exponential decay after the KL peak [13], it would be possible to quantify the late-cycle soot oxidation rate by extracting the half-life value of the decay curve.

This analysis was done by fitting an exponential equation to the experimental data shown in Figure 5.

Once the exponential KL curve is obtained, the half-life time, $t_{1/2}$, is given by Equation 3:

$$KL = a \cdot e^{\frac{-\ln(2)\cdot x_{CAD}}{t_{\frac{1}{2}}}} \qquad (3)$$

where *a* is a constant and x_{CAD} is the crank angle position aTDC in CAD. Thus, the half-life time of KL, $t_{1/2}$ KL, is defined as the time required for the initial soot concentration volume to be oxidized up to its half value. It is an estimate of the soot oxidation rate: the lower the $t_{1/2}$ KL, the higher the oxidation rate.

Figure 6 shows the temporal evolution of the experimental ACT^{-1} for the 2000 rpm and 2 bar BMEP case with an injection pressure of 400 bar. The curve represents the average of 100 cycles and its standard deviation. As for the optical thickness analysis, only the late-cycle part of the curve is selected for studying the soot oxidation rate, i.e. from the EoI up to EoC. The experimental ACT^{-1} depends on in-cylinder air density, ρ_a, injection velocity, u_0, and oxygen molar fraction, $[O_2]$, as follows [22]: Thus, ACT^{-1} can be considered as a 'mixing capability' tracer.

$$ACT^{-1} = \frac{\rho_a^{0.5}\cdot u_0\cdot [O_2]^{0.5}\cdot \phi_0^{-1}}{K} \qquad (4)$$

To quantify the mixing capability related with soot oxidation, exponential decay functions were also used to fit ACT^{-1} curves.

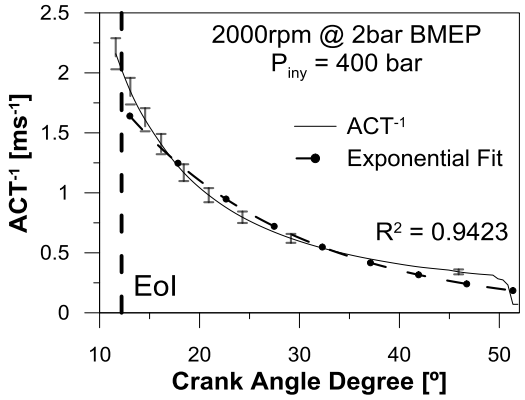

Figure 6. ACT^{-1} trace for the P_{inj} = 400 bar case at point 2000rpm@2bar BMEP and its exponential fit

By definition, the half-life time of exponential ACT^{-1} curve is given by:

$$ACT^{-1} = b \cdot e^{\frac{-\ln(2) \cdot x_{CAD}}{t_{\frac{1}{2}}}} \qquad (5)$$

where *b* is a constant and x_{CAD} is the crank angle position aTDC in CAD. Thus, the half-life time of ACT^{-1}, $t_{1/2}$ ACT^{-1}, is defined as the time required for the mixing capability to be the half of its initial value. It is an estimate of the rate of 'mixing capability'.

4. RESULTS AND DISCUSSION

This section presents the study of soot oxidation with variation in injection pressure, intake air density and temperature in a production four-cylinder direct injection light-duty diesel engine.

4.1. Effect of injection pressure on late cycle soot oxidation

Injection pressure has a well-known effect on the diesel combustion process. An increase in injection pressure produces an increase in the total air entrained into the fuel spray upstream of the lift-off length (LOL), which results in a decrease in the equivalence ratio at the lift-off length (ϕ_{LOL}) and thus, a decrease in soot formation [14].

A reduction in exhaust soot emissions is thereby attained when injection pressure is increased. During the current research, two tracers were used to analyze the impact of the injection pressure on the soot oxidation processes: on the one hand, the half-life time for the optical thickness is proposed with the aim of evaluating the reduction in soot content after the EoI and, on the other hand, to evaluate the mixing capability and its effect on the combustion process (and therefore on soot emissions), the half-life time for ACT^{-1} is used. Thus, in this sub-section, results for variation of the injection pressure from 400, 600 and 800 bar at the 2000rpm@2bar BMEP operating point are presented, while the rest of engine settings were held constant. As explained previously, the temporal evolutions of KL and ACT^{-1} were recorded for 400 cycles. Exponential decay functions were used to fit KL and ACT^{-1} after the EoI, as already explained in section 3.3.

Based on the injection pressures tested, the crank angle degree intervals to perform the fit are different for each decay curve. These intervals are represented in Table 3.

	KL		ACT^{-1}	
P_{inj} [bar]	Interval fitting [CAD]	R^2 - values [-]	Interval fitting [CAD]	R^2 - values [-]
400	13 - 43	0.9346	13 - 50	0.9423
600	14 - 43	0.9357	13 - 51	0.9211
800	15 - 43	0.9461	13 - 53	0.9479

Table 3. Intervals used and corresponding R^2- values for the exponential fits to KL and ACT^{-1} for the injection pressure sweep at point 2000rpm@2bar BMEP

Each interval was selected based on a detailed study of the curve shapes. In these tests, the onset of the exponential fits starts after the EoI (approximately the maximum KL) which was between 13 – 15 CAD aTDC depending on the injection pressure considered. The end of the intervals for the exponential fit ranges from 43 to 53 CAD

aTDC, where the KL and ACT^{-1} profiles approach zero. The R^2-values shown in Table 3 indicate a proper accuracy level of each exponential fit, ranging from 0.93 up to 0.98.

Figure 7 presents the average half-life times for KL, $t_{1/2}$ KL, as well as their corresponding standard deviation, for the different injection pressures swept. As others researchers found in the literature [10, 15], an increase in the injection pressure leads to a decrease in soot. In particular, it is possible to state that the half-life time of KL decreases with an increase in the injection pressure.

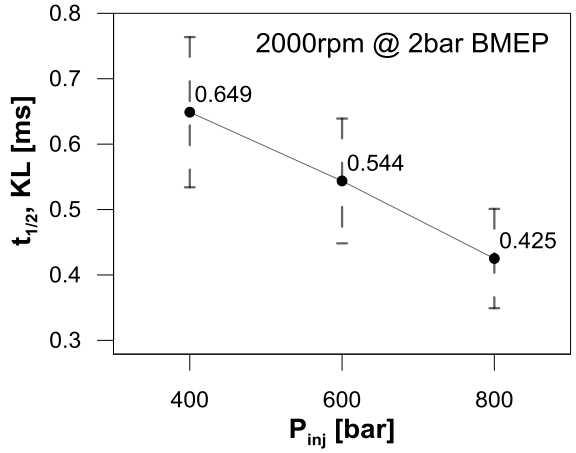

Figure 7. Half-life time of KL, $t_{1/2}$ KL, calculated for the injection pressure sweep at point 2000rpm@2bar BMEP

Figure 8 shows the results of half-life times of ACT^{-1} (average value and its standard deviation) for the injection pressure sweep. The half-life times of the ACT^{-1}, $t_{1/2}$ ACT^{-1}, decrease when the injection pressure is increased. Considering constant in-cylinder ambient density and oxygen concentration between the different injection pressure cases, a higher injection pressure produces an increase in the total air entrained into the fuel, which results in an improvement in the soot oxidation process. In addition, the momentum produced by the spray in the case of high injection pressure (P_{inj}= 800bar) is higher than with low injection pressure (P_{inj}= 400bar). Thus, an increase in the movement of the in-cylinder air environment is achieved due to the higher momentum of the spray. The increased air movement affects soot oxidation by enhancing the mixing process during the late cycle period, and therefore the soot oxidation rate is increased when the injection pressure is increased [15]. All these phenomena translate into a lower time to burn the same amount of injected fuel when comparing the tests with higher injection pressure to those with lower injection pressure.

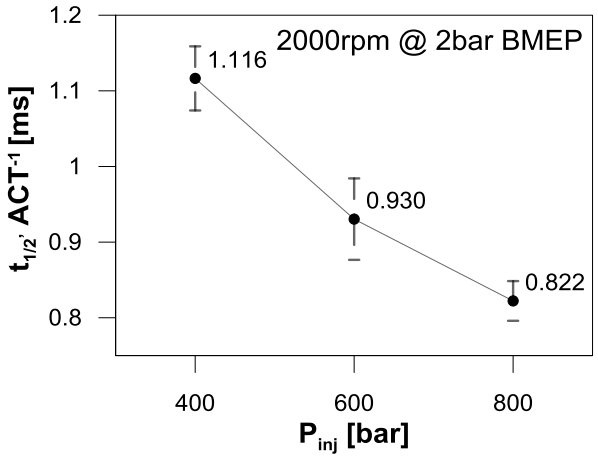

Figure 8. Half-life time of ACT^{-1}, $t_{1/2}$ ACT^{-1}, calculated for the injection pressure sweep at point 2000rpm@2bar BMEP

Considering Figures 7 and 8, it can be stated that similar trends were attained for both half-life times. Thus, the $t_{1/2}$ ACT^{-1} can be used to explain the soot oxidation process, as will be seen in subsection 4.4.

4.2. Effect of ambient density on late cycle soot oxidation

In this sub-section, soot oxidation will be analyzed for varying ambient density, while maintaining constant the rest of the engine settings. The values of ambient density were defined considering the minimum, middle and maximum intake pressure produced by the turbocharger for each operating point. In particular, for the 2000 rpm and 2 bar BMEP operating conditions, the values of ambient density selected are 18.1, 22.0 and 25.6 kg/m^3. As in the injection pressure sweep, the temporal evolution of KL and ACT^{-1} were recorded for 400 cycles, and the same processing methodology was followed. Exponential decay functions were used to fit KL and ACT^{-1} after the EoI.

Figures 9 and 10 show the half-life time for KL and ACT^{-1}, respectively. The average values for the two tracers are represented together with their corresponding standard deviations. The chosen crank angle degree intervals for the fitting and R^2-values are presented in Table 4.

	KL		ACT^{-1}	
ρ_{TDC} [kg/m^3]	Interval fitting [CAD]	R^2 - values [-]	Interval fitting [CAD]	R^2 - values [-]
18	18 - 45	0.9221	16 - 52	0.9034
22	17 - 42	0.9402	16 - 51	0.9235
26	17 - 42	0.9544	17 - 51	0.9654

Table 4. Intervals used and corresponding R^2- values for the exponential fits to KL and ACT^{-1} for the ambient density sweep at point 2000rpm@2bar BMEP

Figure 9 shows the average and standard deviation of the half-life time of KL, $t_{1/2}$ KL. If the ambient density is decreased, the half-life time of KL is larger. A decrease in

ambient density produces larger combustion duration and slower decay at the late part of the profile due to slower combustion development [24]. This fact implies poorer soot oxidation and therefore the half-life time of KL increases, as shown in Figure 9.

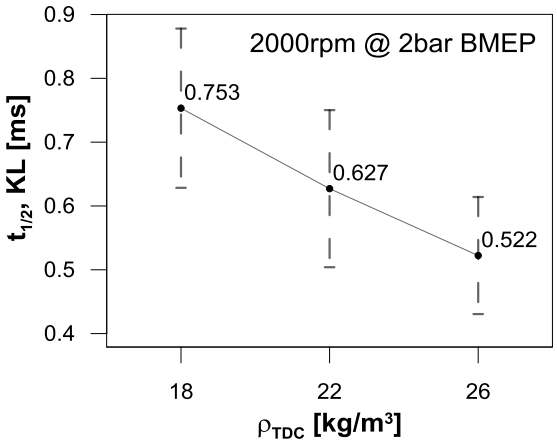

Figure 9. Half-life time of KL, $t_{1/2}$ KL, calculated for the ambient density sweep at point 2000rpm@2bar BMEP

Figure 10 presents the average values and standard deviations of the half-life time of ACT^{-1}, $t_{1/2}$ ACT^{-1}, for the different ambient densities swept. When the ambient density was increased, the air/fuel mixing process was improved, which implies shorter $t_{1/2}$ ACT^{-1}.

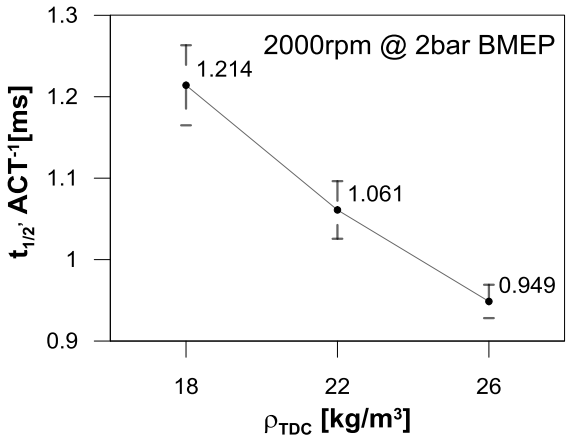

Figure 10. Half-life time of ACT^{-1}, $t_{1/2}$ ACT^{-1}, calculated for the ambient density sweep at point 2000rpm@2bar BMEP

4.3. Effect of intake air temperature on late cycle soot oxidation

The effect of intake air temperature variation on soot oxidation will be investigated in this sub-section. Intake air temperature values have been varied maintaining the ambient density at TDC at 22 kg/m^3. The intake air temperature sweep ranged from 303 to 333 K. The lower limit is delimited by the coolant temperature of the intercooler, whereas the upper limited is defined considering the maximum intake air temperature downstream of the compressor (intercooler switched off). As in both previous sweeps, the temporal evolution of KL and ACT^{-1} were recorded for 400 cycles and the same processing methodology was followed. Exponential fits of KL and ACT^{-1} after the EoI were performed. The half-life times for the two parameters are presented in Figures 11 and 12, and the selected intervals for the fits and the R^2- values are given in Table 5.

	KL		ACT^{-1}	
T_{in} [K]	Interval fitting [CAD]	R^2 - values [-]	Interval fitting [CAD]	R^2 - values [-]
303	16 - 46	0.9482	15 - 45	0.9309
313	15 - 46	0.9601	15 - 45	0.9469
323	15 - 47	0.9832	16 - 47	0.9533
333	16 - 48	0.9508	15 - 49	0.9620

Table 5. Intervals used and corresponding R^2- values for the exponential fits to KL and ACT^{-1} for the intake air temperature sweep at point 2000rpm@2bar BMEP

As other researches indicate in the literature [10, 16], the soot oxidation process is improved with higher intake air temperature. In particular, the half-life time of KL, $t_{1/2}$ KL, decreases when the intake air temperature was increased. This behavior can be observed in Figure 11. It is important to note that the half-life times of KL are very similar due to the small variation in the values of intake air temperature (just 40 K of variation, i.e. less than 15%).

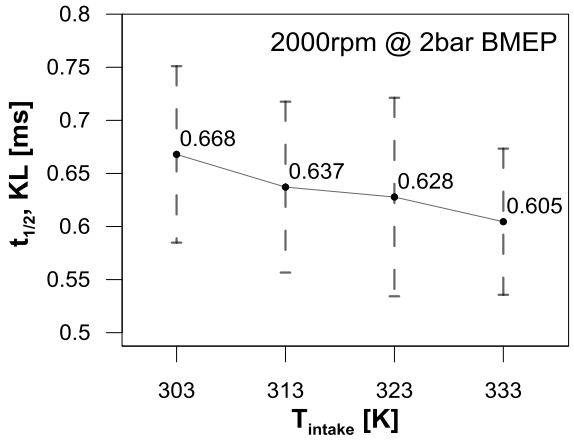

Figure 11. Half-life time of KL, $t_{1/2}$ KL, calculated for the intake air temperature sweep at point 2000rpm@2bar BMEP

Figure 12 shows the average values and standard deviations of the half-life time of ACT^{-1}, $t_{1/2}$ ACT^{-1}, for the different intake air temperatures. When the intake air temperature was increased, a shorter $t_{1/2}$ ACT^{-1} was obtained, showing that the mixing capability seems to increase. The authors haven't found any easy explanation to this

increase in mixing capability caused by the intake air temperature increase. However, it should be taken into account that the observed variation is quite small.

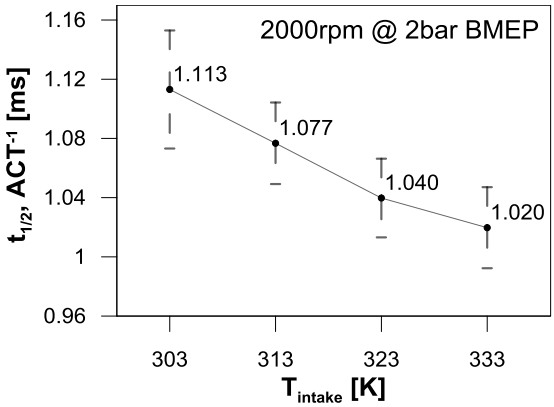

Figure 12. Half-life time of ACT^{-1}, $t_{1/2}$ ACT^{-1}, calculated for the intake air temperature sweep at point 2000rpm@2bar BMEP

4.4. Analysis of late cycle soot oxidation Half-Life times

Once the half-life times of KL and ACT^{-1} have been analyzed separately for each parameter sweep at one operating condition (2000rpm@2bar BMEP), this section aims to relate all three parameters under the two operating conditions (both at low load: 2 and 5 bar BMEP) tested. In particular, the relationship between the mixing capability on the soot oxidation process will be analyzed and described.

Figure 13 shows the average half-life time of KL versus the average half-life of ACT^{-1} at 2000rpm and 2 bar BMEP. Results from different injection pressures, air densities and intake air temperatures (i.e. the three sweeps already shown in the previous subsections) are presented. For this engine operating point and these parameter sweeps, the R^2-values were already illustrated in the previous subsections (Tables 3, 4 and 5), showing an acceptable accuracy. Therefore, the robustness of the methodology is demonstrated. Thus, when the mixing process is inhibited due to a decrease in the

injection pressure, air density and/or intake air temperature, the soot oxidation is poorer and therefore the $t_{1/2}$ KL is larger. Trying to evaluate how the $t_{1/2}$ ACT^{-1} parameter correlates with the soot oxidation process ($t_{1/2}$ KL), a linear fit was performed to the 10 different cases, and a reasonable result is obtained (see Figure 13).

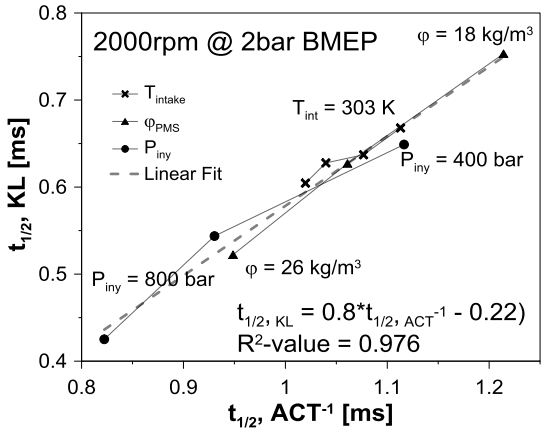

Figure 13. Relationship between half-life times of the KL and ACT^{-1} at 2000rpm@2bar BMEP for the different sweep: injection pressure, ambient density and intake air temperature

Figure 14 shows the average half-life time of KL versus the average half-life time of ACT^{-1} at 2000 rpm and 5 bar BMEP. As in the previous case, all the results from the different sweeps are presented together. For these engine conditions, the corresponding R^2-values are shown in Table 6. The same methodology was followed as in the 2 bar BMEP operating point. Both half-life times trends were similar to those obtained at the 2 bar BMEP point. In general, the inhibition of the mixing process produced by a reduction in the injection pressure and/or a deterioration of the in-cylinder conditions (low density, low intake air temperature) correlates with a poorer oxidation process. With the objective of quantifying this relationship, a linear fit was performed to the 10 different cases, also obtaining a reasonable accuracy level.

2000rpm@5bar - KL					
P_{iny} [bar]	R^2 - values [-]	ρ_{TDC} [kg/m^3]	R^2 - values [-]	T_{in} [K]	R^2 - values [-]
400	0.9751	19	0.9950	303	0.9576
600	0.9916	24	0.9818	313	0.9762
800	0.9832	28	0.9639	323	0.9410
				333	0.9649
2000rpm@5bar - ACT^{-1}					
P_{iny} [bar]	R^2 - values [-]	ρ_{TDC} [kg/m^3]	R^2 - values [-]	T_{in} [K]	R^2 - values [-]
400	0.9912	19	0.9668	303	0.9657
600	0.9819	24	0.9755	313	0.9710
800	0.9739	28	0.9741	323	0.9837
				333	0.9763

Table 6. R^2- values for the exponential fits to KL and ACT^{-1} for the injection pressure, ambient density and intake air temperature sweeps at point 2000rpm@5bar BMEP

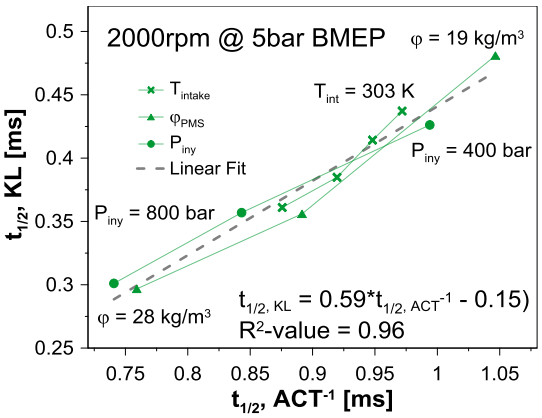

Figure 14. Relationship between half-life times of the KL and ACT^{-1} at 2000rpm@5bar BMEP for the different sweeps: injection pressure, ambient density and intake air temperature

To provide a more general approach and considering the reasonable linear agreement between $t_{1/2}$ KL and $t_{1/2}$ ACT^{-1} for the two operating conditions tested, both half-life times (for KL and ACT^{-1}) should be related by the equation below:

$$t_{\frac{1}{2}KL} = A \cdot t_{\frac{1}{2}ACT^{-1}} - B \quad (6)$$

Figure 15 presents the experimental half-life time versus the simulated half-life time (from Equation 6). The coefficients A and B were adjusted for the two operating conditions separately, using the 10 different tests performed at each of them. The values of A and B coefficients are 1.01 and -0.48, respectively. In view of the figure, it can be said that the differences between the experimental and simulated half-life times, even if they are inside acceptable limits, is not perfect. A possible explanation is that soot oxidation is an extremely complex process that might not be governed solely by the mixing process.

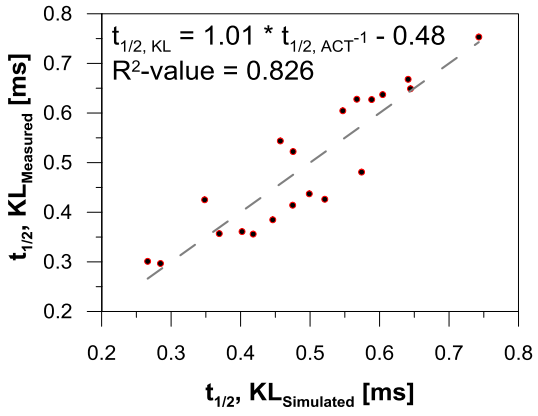

Figure 15. Experimental half-life time of KL versus the simulated half-life time of KL (from Equation 6) for all the tests performed at the two operating conditions

Thus, to improve the prediction of the current model (Equation 6), additional parameters are surely needed. It is well known that in-cylinder gas temperature should have a considerable impact on soot oxidation [9]. Figure 16 presents the KL half-life time error, defined as the experimental results minus the simulated ones, as a function of the average bulk gas temperature. This average was calculated considering the bulk gas temperature values in the crank angle degree range previously used to fit the ACT^{-1} half-life time. It is worth noting that this way to proceed seems reasonable, since the

range considered for computing the average temperature corresponds to the range where soot oxidation is under analysis.

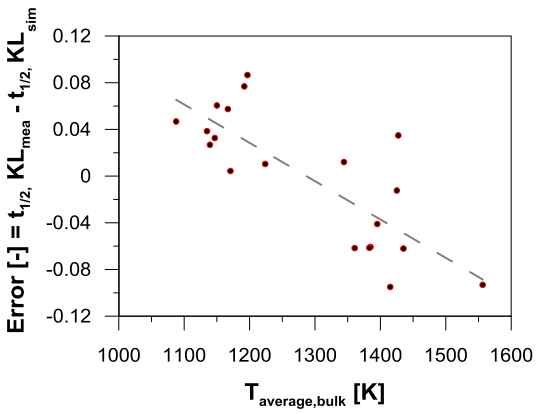

Figure 16. Correlation between errors defined as experimental KL half-life time minus simulated KL half-life time (from Equation 6) and average bulk gas temperature

Based on this figure, it can be seen that the error of the current model is not at all random, since it correlates quite well with the average bulk gas temperature. Besides, if correctly analyzed, the correlation makes the most sense: on the one hand, when the bulk gas temperatures are high, the model is overestimating the KL half life time (i.e. the error is negative), which means that it is underestimating the oxidation process. This result illustrates that this underestimation is because the model is not taking into account this higher bulk gas temperature, which enhances the oxidation process. On the other hand, when the bulk gas temperatures are low, the model is underestimating the KL half life time (i.e. the error is positive), implying that it is overestimating the oxidation process. The reason for this overestimation is that the model is not taking into account the lower bulk gas temperature, which hinders the oxidation process.

Thus, a new model was built, including the two significant parameters previously presented (‘mixing capability’ and average bulk gas temperature), to better explain the soot oxidation process, which has the form shown in Equation 7:

$$t_{\frac{1}{2}KL} = C \cdot t_{\frac{1}{2}ACT-1}^{D} \cdot (T_{bulk}/10^3)^E \quad (7)$$

Figure 17 shows the experimental KL half-life time versus the simulated one (with Equation 7). The coefficients C, D and E were adjusted for the two different operating conditions (2 and 5 bar BMEP). The values of C, D and E coefficients are 0.66, 1.62 and -1.05, respectively. From the figure, it can be observed that this new model is significantly more accurate than the previous one. In this sense, the present work confirms the relevance of the 'mixing capability' and temperature in the soot oxidation process. It is interesting to note that to determine both soot oxidation tracers, 'mixing capability' and average bulk temperature, it is only necessary to have the heat release and the injection rate profiles, which can be obtained quite easily in real engines.

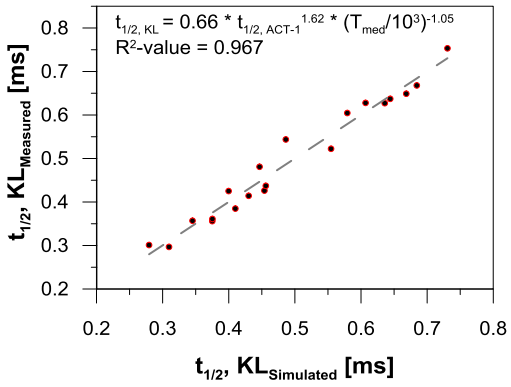

Figure 17. Correlation between half-life of the measured KL and the simulated one (from Equation 7) for all the tests performed at the two operating conditions

5. Conclusions

The main objective of this work was to define a simplified methodology to evaluate in-cylinder soot oxidation under 'real' engine conditions. In particular, the influence of the in-cylinder mixing process was studied. The experimental measurements were made in a production light-duty diesel engine by varying the injection pressure, ambient density

at TDC and intake air temperature. In particular, experimental and theoretical parameters were used to perform the study. On the hand, the soot oxidation process was characterized with the half-life time of an exponential fit applied to the optical thickness (KL) signal. KL was obtained by applying the two color method using a dedicated optoelectronic pyrometer. On the other hand, a mixing capability estimator (ACT^{-1}) was also calculated. An exponential fit was applied to the temporal evolution of ACT^{-1}. This tracer was obtained with simulated injection rates and experimental heat release measurements. The conclusions of the study can be summarized as follows:

- The half-life time of ACT^{-1} was increased, and therefore the 'mixing capability' was poorer, with a decrease in the injection pressure, ambient density and/or air intake temperature. In the case of injection pressure, lower values of injection pressure produce lower injection velocity and thus, a worsening in the mixing process. Concerning the ambient density at TDC, when the ambient density was increased the air/fuel mixing process was improved. Finally, if the intake air temperature was higher, the mixing process was observed to be also better.
- A 0D model based on experimental measurements was developed to obtain the half-life time of KL and the half-life time of ACT^{-1}. As expected, the 'mixing capability' cannot fully explain a complex phenomenon such as soot oxidation. In this sense, the average bulk gas temperature has been included as an additional tracer in the 0D model, significantly improving the accuracy of the soot oxidation process predictions.

Acknowledgments

The authors acknowledge General Motors Global Research & Development for supporting this research.

References

[1] Benajes J., Martín J., García A., Villalta D, Warey A. In-cylinder soot radiation heat transfer in direct-injection diesel engines. Energy Conversion and Management 106 (2015) 414–427, doi:10.1016/j.enconman.2015.09.059.

[2] Torregrosa, A., Olmeda, P., Martín J., Romero C. A Tool for Predicting the Thermal Performance of a Diesel Engine. Heat Transfer Engineering, 32: 10, 891 - 904, doi: 10.1080/01457632.2011.548639.

[3] Serrano J., Olmeda P., Tiseira A., García-Cuevas L. et al. Importance of Mechanical Losses Modeling in the Performance Prediction of Radial Turbochargers under Pulsating Flow Conditions. SAE Int. J. Engines 6(2):729-738, 2013, doi:10.4271/2013-01-0577.

[4] Benajes J., Novella R., De Lima D., Tribotte P., Quechon N., Obemesser P., Dugue V. Analysis of the combustion process, pollutant emissions and efficiency of an innovative 2-stroke HSDI engine designed for automotive applications. Applied Thermal Engineering 58 (2013) 181-193, doi:10.1016/j.applthermaleng.2013.03.050.

[5] Benajes J., García A., Pastor J.M., Monsalve-Serrano J. Effects of piston bowl geometry on Reactivity Controlled Compression Ignition heat transfer and combustion losses at different engine loads. Energy, Volume 98, 1 March 2016, Pages 64-77, doi.org/10.1016/j.energy.2016.01.014.

[6] Benajes J., García A., Monsalve-Serrano J., Balloul I., Pradel G., An assessment of the dual-mode reactivity controlled compression ignition/conventional diesel combustion capabilities in a EURO VI medium-duty diesel engine fueled with an intermediate ethanol-gasoline blend and biodiesel. Energy Conversion and Management, Volume 123, 1 September 2016, Pages 381-391, doi.org/10.1016/j.enconman.2016.06.059.

[7] Pickett L.M., Siebers D.L. Soot in diesel fuel jets: effects of ambient temperature, ambient density, and injection pressure. Combustion and Flame 138 (2004) 114–135, doi:10.1016/j.combustflame.2004.04.006.

[8] Dec JE. A conceptual model of DI diesel combustion based on laser-sheet imaging. SAE Paper 970873, 1997, doi: 10.4271/970873.

[9] Tree, D.R, Svensson, K. I. Soot processes in compression ignition engines. Progress in Energy and Combustion Science 33 (2007) 272–309, doi:10.1016/j.pecs.2006.03.002.

[10] Arrègle J., Pastor J.V., López J.J., García A. Insights on postinjection-associated soot emissions in direct injection diesel engines. Combustion and Flame 154 (2008) 448–461, doi:10.1016/j.combustflame.2008.04.021.

[11] Heywood, J.B. Internal Combustion Engine Fundamentals. McGraw-Hill Book Co, New York, US, 1988.

[12] Xiaobei C., Hongling J, Zhaowen W. A Numerical Modeling and Experimental Study on Soot Formation for a Direct Injection Diesel Engine. SAE Technical Paper 2008-01-1794, 2008, doi:10.4271/2008-01-1794.

[13] Gallo Y., Simonsson J., Lind T., Bengtsson P., et al., O. A Study of In-cylinder Soot Oxidation by Laser Extinction Measurements During an EGR-Sweep in an Optical Diesel Engine. SAE Technical Paper 2015-01-0800, 2015, doi:10.4271/2015-01-0800.

[14] Dembinski H., Angstrom H. Swirl and Injection Impact on After-Oxidation in Diesel Combustion, Examined with Simultaneous Combustion Image Velocimetry and Two Colour Optical Method. SAE Technical Paper 2013-01-0913, 2013, doi:10.4271/2013-01-0913.

[15] Huestis, E., Erickson, P., and Musculus, M. In-Cylinder and Exhaust Soot in Low-Temperature Combustion Using a Wide-Range of EGR in a Heavy-Duty Diesel Engine. SAE Technical Paper 2007-01-4017, 2007, doi:10.4271/2007-01-4017.

[16] López, J., Martin, J., Garcia, A., Villalta, D. et al. Characterization of In-Cylinder Soot Oxidation Using Two-Color Pyrometry in a Production Light-Duty Diesel Engine. SAE Technical Paper 2016-01-0735, 2016, doi:10.4271/2016-01-0735.

[17] DRIVVEN Stand Alone Direct Injector Driver System User's Manual October 2010. Drivven, INC. 12001 Network Blvd, 110. San Antonio, Texas 78249. Web: www.drivven.com<http://www.drivven.com>

[18] Payri, F., Olmeda, P., Martin, J., and Carreño, R. A New Tool to Perform Global Energy Balances in DI Diesel Engines. SAE Int. J. Engines 7(1):2014, doi:10.4271/2014-01-0665.

[19] Payri F., Pastor J., Garcia J. Contribution to the application of two-colour imaging to diesel combustion. Measurement Science and Technology, vol. 18, no. 8, pp. 2579-2598, 2007, doi:10.1088/0957-0233/18/8/034.

[20] Zhao H., Ladommatos N. Optical diagnostics for soot and temperature measurement in diesel engines. Progress in Energy and Combustion Science, vol. 24, no. 3, pp. 221-255, 1998, doi:10.1016/S0360-1285(97)00033-6.

[21] Hottel H., Broughton F. Determination of True Temperature and Total Radiation from Luminous Gas Flames. Industrial and Engineering Chemistry, vol. 4, no. 2, pp. 166-175, 1932, doi:10.1021/ac50078a004.

[22] Arrègle J., López J.J., García J.M., Fenollosa C. Development of a Zero Dimensional Diesel Combustion Model. Part 1: Analysis of the Quasi-steady Diffusion Combustion Phase. Applied Thermal Engineering, Vol. 23, pp. 1301-1317, doi:10.1016/S1359-4311(03)00079-6.

[23] Payri F., Olmeda P., Martín J., García A. A complete 0D thermodynamic predictive model for direct injection diesel engines. Appl. Energy 88(12)(2011)4632e4641, doi:10.1016/j.apenergy.2011.06.005.

[24] Musculus, P.B. M. Measurements of the influence of Soot Radiation on In-Cylinder Temperatures and Exhaust NOx in a Heavy-Duty DI Diesel Engine. SAE Technical Paper 2005-01-0925, 2005, doi:10.4271/2005-01-0925.

[25] Hottel H. and Broughton, F. P. Determination of True Temperature and Total Radiation From Luminous Gas Flames. Ind. Eng. Chem. Anal. Ed., 4(2), pp. 166-175, 1932, doi:10.1021/ac50078a004.

[26] Vogelin P. Experimental investigation of multi-in-cylinder pyrometer measurements and exhaust soot emissions under steady and transient operation of a heavy-duty Diesel engine. SAE Technical Paper 131ICE-0145, 2013, doi:10.4271/2013-24-0177.

[27] Desantes J.M., Pastor J.V., García-Oliver J.M., Pastor J.M. A 1D model for the description of mixing-controlled reacting diesel sprays. Combust. Flame 156 (2009) 234e249, doi:10.1016/j.combustflame.2008.10.008.

[28] Pastor J.V., Lopez J.J., Garcia J.M., Pastor J.M. A 1D model for the description of mixing-controlled inert diesel sprays. Fuel 87 (13e14) (2008) 2871e2885, doi:10.1016/j.fuel.2008.04.017.

[29] Payri F., Pastor J.V., García J.M., Pastor J.M. Contribution to the application of two-color imaging to diesel combustion. Meas. Sci. Technol. 18 (2007) 2579–2598, doi:10.1088/0957-0233/18/8/034.

[30] Musculus M.P.B., Singh S., Reitz R.D. Gradient effects on two-color soot optical pyrometry in a heavy-duty DI diesel engine. Combustion and Flame 153 (2008) 216–227, doi:10.1016/j.combustflame.2007.10.023.

Abbreviations

ACT: Apparent Combustion Time

CA50: Crank Angle at 50% mass fraction burned

EoC: End of Combustion

EoI: End of Injection

EVO: Exhaust Valve Open

FWHM: Full Width al Half Maximun

HT: Heat transfer

HRL: Heat Release Law

IVC: Inlet Valve Close

$I_{b,\lambda}$: Spectral Intensity of Black Body

I_{soot}: Spectral Intensity

KL: Optical Thickness

LOL: Lift-off Length

P_{in}: Intake Pressure

P_{inj}: Injection Pressure

PM: Particulate matter

RoHR: Rate of Heat Release

SoI: Start of Injection

T_{in}: Intake Temperature

u_0: Injection velocity

VGT: Variable Geometry Turbocharger

α: Absorptivity

ε: Emissivity

λ: Wavelength

θ: Spray Cone Angle

ρ_0: Density

ϕ_0: Equivalence Ratio

Appendix

1. Uncertainty of two-color pyrometry: flame transparency

In the past, the two-color pyrometry method has been used to evaluate the sooting processes from diesel engine flames [9]. A detailed description of the two-color method can be found in [25]. In this particular research, this optical method was applied in a production engine where the room for optical access to the combustion chamber was limited. The recorded signal in this case represented the spatially integrated information of a three dimensional complex phenomenon, which is characterized by significant spatial gradients of equivalence ratio and temperature along with the combination of reactive and non-reactive zones as well as different absorption coefficients and soot particle densities along the line-of-sight [26]. Additionally, this two-color pyrometry method has some uncertainties due to fouling in the optical device from in-cylinder soot or from occlusion of the field of view by geometric factors of the measurement system [16].

In order to analyze the radiation evolution inside the flame, it is necessary to have the spatial distribution of the temperature and soot in the flame. The local temperature values have been achieved by means of an in-house 1D spray model, DICOM described by Desantes et al. in [27] and Pastor et al. in [28]. The main objective of using this model is to obtain a local equivalence ratio distribution and, therefore, a flame temperature map. The 1D spray model is based on two main assumptions: on the one hand, that the fuel is injected with a uniform velocity at the whole nozzle section and, on the other hand, that the momentum exchange of the fuel with the surrounding air

leads to an increase in the width of the spray as the axial distance increases. The radial growth of the spray is determined by its cone angle, which is the only tuning parameter of the model. The entire spray domain is divided axially in a certain number of cells (i.e. a 1D grid) that occupy the whole spray cross section, and the model solves momentum and fuel mass conservation equations for the spray in this grid. To simplify the spatial description of both properties, self-similar Gaussian profiles are assumed, which makes it possible to transform a 2D problem (if symmetry is assumed) into a 1D one. In a first step, for each dx-sized cell, only the on-axis properties are solved. Within each cell, the amount of fuel mass evaporated at a given time step is calculated based on the amount of energy introduced in the cell by the entrained air. In a second step, the radial distribution of properties can be obtained by using the corresponding self-similar profiles.

The inputs needed for the model are the in-cylinder thermodynamical conditions (pressure and density), the injection rate, the characteristics of the nozzle and the spray cone angle. This last parameter is the unique parameter to be adjusted. Once all this information is available, the model solves the general conservation equations for axial momentum and fuel mass in terms of the on-axis (i.e. center line) values of velocity and species mass fraction.

Thus, two operating conditions were analyzed for clarifying the flame transparency drawback presented in two-color method, one representative of low load (2000rpm@2bar BMEP) and other representative of high load (1500rpm@14bar BMEP). All relevant variables of these engine conditions are presented in Table 7. Figure 18 shows the experimental (continuous line) and modelled (dashed line) RoHR for both operating conditions. The experimental data were processed with the in-house 0D combustion analysis model CALMEC and the modeled data were obtained with the

1D spray code, DICOM. The spray cone angle has been adjusted to fit as much as possible the modeled profile with the experimental one. In this case a $\theta = 23^{\circ}$ has been used for both conditions. This value for the spray cone angle is quite representative of diesel sprays. Thus, it is possible to observe that the modelled curves are quite similar to the experimental curves.

Speed [rpm]	bmep [bar]	Intake press. [bar]	Exhaust press. [bar]	Air mass [kg/min]	Fuel Flow [kg/min]	P_{inj} [bar]	Density [kg/m^3]	Intake Temp. [K]
2000	2	1.165	1.294	2.33	0.039	450	20.5	318
1500	14	1.732	2.191	2.29	0.140	1050	25.7	

Table 7. Experimental engine operating conditions used to evaluate some uncertainties of the optical technique

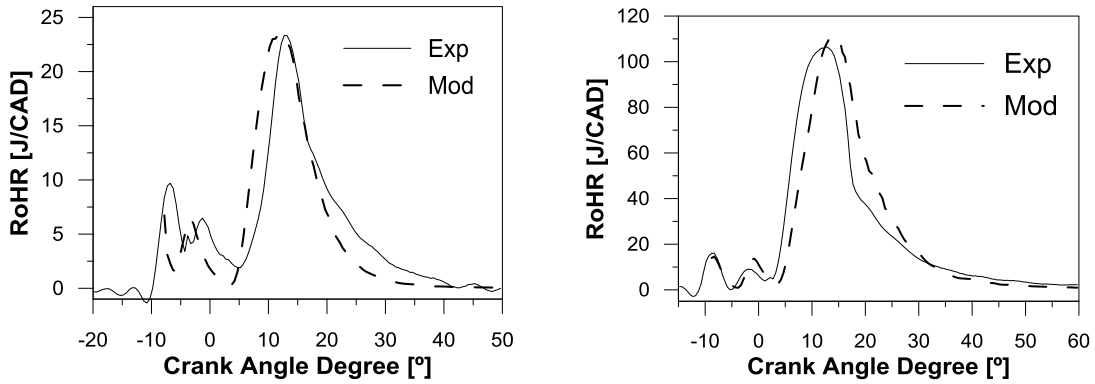

Figure 18. An experimental and modelled RoHR for (left) 2000rpm@2bar BMEP point and (right) 1500@14bar BMEP point. The dashed line indicates the modelled data and the continuous line the experimental data.

Figure 19 shows the spatial temperature distribution obtained by DICOM for the 2000rpm@2bar BMEP at 2ms after start of Injection (SoI). The modelled temperature distribution is represented as a function of the axial (X-axis) and radial (Y-axis) positions. In the figure three different zones can be observed: (1) the dashed line is the stoichiometric surface, where the maximum temperatures are reached; in this location the fuel diffused from the inner part of the flame reacts with oxygen from the outer part. (2) The inner zone, which corresponds to the rich side of the flame; this region consists

of partially oxidized fuel, combustion products and soot. (3) The outer part, which is the lean side of the flame; in this region fresh air and combustion products are present.

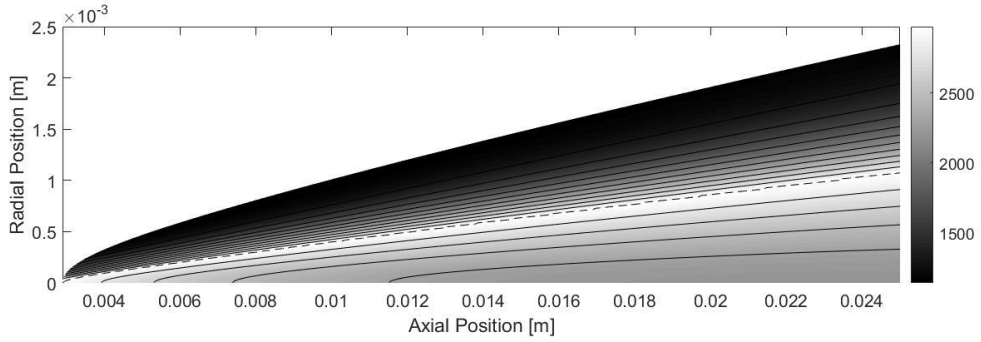

Figure 19. Modelled temperature distributions for 2000rpm@2bar BMEP at 2ms after SoI. The dashed line shows the stoichiometric surface

In addition, it is assumed that soot is only present in the inner part of the flame, as it is totally oxidized by the OH present on the reaction zone [8]. A physical description of the soot distribution would demand a soot model, which is not easy to derive and it is out of the scope of the present research. Two radial soot distributions have been evaluated in this work: a constant and a linear soot distribution profile [7].

Figure 20 presents the modeled combustion temperature and soot (constant and linear) distribution for a particular axial position. The flame is divided radially into discrete flame elements with their corresponding value of temperature and other properties. To analyze the radiation propagation inside the flame both the emission and the absorption processes will be considered.

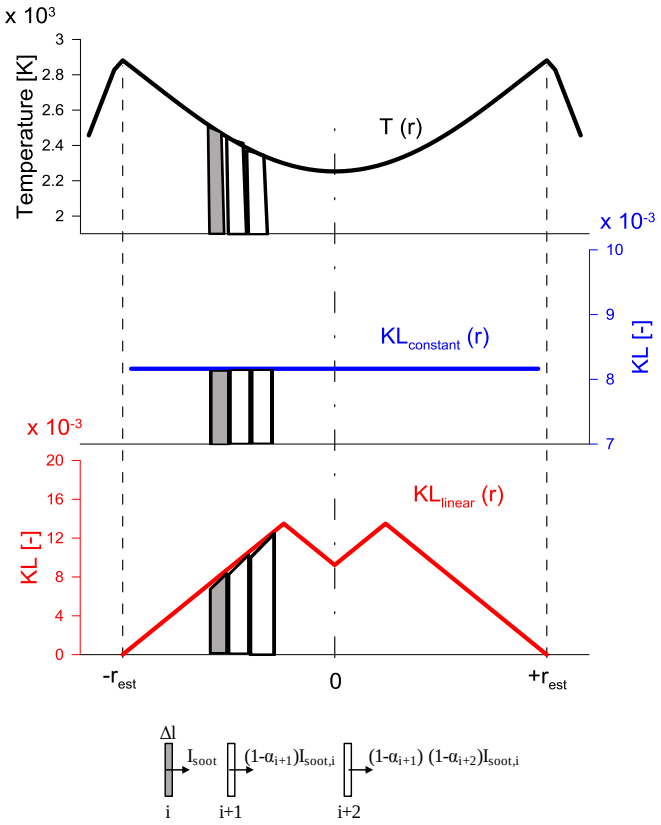

Figure 20. Flame transparency model. The image shows the radial propagation of the radiation emitted by the i-th element through the flame up to the radiation sensor (located on the right of the figure) at 2000rpm@2 bar BMEP

Considering the temperature and soot distributions, the radiation propagation process inside the flame is based on the following:

- Radiation is propagated along lines parallel to the flame main symmetry plane.
- The spatial distribution of the local gas temperature is assumed to be equal to the soot temperature. In this case, the flame temperature is calculated by the spray model.
- Both a uniform and a linear KL radial distribution will be considered.
- Soot is assumed to be completely oxidized at the flame stoichiometric surface.

For the calculation, a similar scheme proposed by Payri et al. [29] is followed. The radiation path is divided into *n* elements with the same thickness. Each element *i* has its temperature T_i and optical thickness KL_i. So, considering the proposed soot distributions it can be stated that:

$$KL = \sum_{i=1}^{n} KL_i \qquad (8)$$

The radiation emitted by each element can be calculated as:

$$I_{soot,i}\,(\lambda, T_i, KL_i) = \varepsilon_{\lambda,i} I_{b,(\lambda,T_i)} \qquad (9)$$

The radiation received by the sensor (which is located on the right of Figure 20) at each wavelength is the addition of the $I_{soot,i}$ of each flame element, taking into account its corresponding attenuation.

$$I_{soot,\lambda} = \sum_{i=1}^{n} \left[\varepsilon_{\lambda,i} I_{b,(\lambda,T_i)} \cdot \prod_{j=i+1}^{n} \left(1 - \alpha_{\lambda,j}\right)\right] \qquad (10)$$

where for an element *j* the absorption is defined by the spectral absorptivity as follows (considering Kirchhoff's law):

$$\alpha_{\lambda,j} = \varepsilon_{\lambda,j} \qquad (11)$$

Once the radiation model is defined, it is used, together with the modeled combustion temperature and the assumed soot profiles, to evaluate the two color method uncertainty in terms of KL due to the line-of-sight limitation. In particular, two operating conditions have been measured with the optoelectronic pyrometer, 2000rpm@2bar BMEP and 1500rpm@14bar BMEP.

For the 2 bar BMEP condition, the experimental KL obtained was 0.4. At these conditions a temperature gradient of 505K, between the temperature at stoichiometric

conditions in the radial position and the spray center line temperature, was predicted by DICOM, which seems a realistic value. For KL, two distribution profiles were proposed as shown in Figure 20: constant soot distribution profile (blue continuous line) and linear soot distribution profile (red continuous line). For both profiles, the experimental value of KL was used to split it radially in such a way that the average value of KL corresponds to the measured value. As a result, the radiation model indicates that the value of KL should be 0.335 for the constant soot distribution profile and 0.344 for the linear soot distribution profile. These results imply a reduction of 16% and 14%, respectively, compared to the experimental value obtained by means of the two color method (KL=0.4). In addition, these results are consistent with the conclusion obtained by Payri et al. [29] and Musculus et al. [30], who also calculated a reduction of 20 % in KL considering the line-of-sight uncertainty.

Following the same methodology, the 1500rpm@14bar BMEP point was analyzed. For this engine condition, the experimental value of KL was 2 and the temperature gradient obtained by the spray model between the stoichiometric zone and the spray center line zone was 616 K. In this case, the model predicts a KL value of 1.21 for the constant soot distribution profile and 1.25 for the linear soot profile and, consequently, a 39% and 37% (respectively) of reduction in KL was obtained with respect to the experimental value. A large error was also found by Musculus et al. in [30]. Line-of-sight gradients (600 K) caused a reduction in the two color method KL value approximately 50%. It is also important to note that both models (constant and linear soot distribution) provide very similar results. It indicates that the selection of soot distribution shape is not very important for modelling KL, at least in the operating conditions analyzed in this study.

As a conclusion, the selected model for evaluating the flame transparency uncertainty seems to be consistent with the literature. Regarding the results obtained by the two color method, it is possible to state that the higher the sooting operating conditions, the higher the uncertainty. For this reason, the selected engine operating conditions for this work were the low load operating points of 2 and 5 bar BMEP.